Available online at www.sciencedirect.com
SCIENCE DIRECT
Polymer 47 (2006) 5174–5181
polymer
www.elsevier.com/locate/polymer

Large tensile deformation behavior of PC/ABS alloy

Qin-Zhi Fang, T.J. Wang *, Hui-Min Li

Department of Engineering Mechanics, MOE Key Laboratory for Strength and Vibration, Xi'an Jiaotong University, Xi'an 710049, China

Received 25 November 2005; received in revised form 10 April 2006; accepted 27 April 2006
Available online 2 June 2006

Abstract

Large tensile deformation behavior of the alloy of polycarbonate (PC) and acrylonitrile butadiene styrene (ABS) are experimentally investigated in this paper. Based on the adaptations of digital image correlation (DIC) method suitable for large inhomogeneous deformation in three dimensions, a new displacement measurement system is developed. Using the new displacement measurement system, we obtain the displacement fields in PC/ABS alloy. Such that variations of the strain and strain rate during tension process, and the true stress strain curves for PC/ABS alloy are derived. Also, volume variation of PC/ABS alloy is also discussed. Moreover, in situ scanning electron microscopic (SEM) observation is carried out to study the micro-mechanism of large inhomogeneous deformation of PC/ABS alloy. It is seen that contraction rate of specimen thickness is bigger than that of the width of specimen during plastic deformation. The axial tensile strain rate is much higher in the necking region. It should be noted that the local volume increases with the increase of axial true strain to a certain value, after that it decreases. Initiation and growth of crazes are the main mechanism of tensile deformation of PC/ABS alloy after yielding.
© 2006 Elsevier Ltd. All rights reserved.

Keywords: Thermoplastics; Large strain measurement; Digital image correlation

1. Introduction

It is well-known that polymers are being widely used in a number of critical structures, such as automobiles, aircraft, spacecraft, pressure vessels and pipes, etc. Modeling and predicting the behavior of these structures made of polymers require the knowledge of mechanical response of the materials. However, studies on the deformation and fracture of polymers are still in its infancy compared to metals, and much of the necessary theoretical and experimental frameworks are not yet fully developed for polymers even though extensive works have devoted to this field [1–6]. It is shown that in situ observation of the micro-mechanism of deformation has great assistance to understand the tensile deformation behavior of polymer [7]. The effect of strain rate on the properties of polymer has been paid much attention in recent years [8,9].

Large deformation behavior is fundamental mechanical property of ductile polymers. Accurate large deformation measurement is the basis of establishing the constitutive relations of polymers. Usually, necking in the polymeric specimen occurs at relatively small strain, which results in the inhomogeneous deformation of polymers. In this case, the validity of traditional extensometers is questionable or useless. So, how to evaluate the large inhomogeneous deformation of polymers is still an open problem and alternate methods is urgently required.

In the past two decades, extensive works have been devoted to measure the large tensile deformation of polymers and several methods are developed. Buisson and Ravichandar [10] applied finely spaced grid lines to the surface of rectangular bar-type polycarbonate (PC) specimens, and calculated the axial and transverse displacement gradient at points along the specimen centerline by fitting polynomials to the grid line displacements. Tracking the axial position of transverse grid lines printed on the surface of rectangular bar-type specimens of polypropylene and styrene butadiene elastomer. Haynes and Coates [11] measured the true axial strain from the relative displacement between neighboring grid lines and calculated the true axial stress by assuming constant volume deformation. G'Sell et al. [12] calculated the true stress–strain behavior of several glassy and semi-crystalline polymers by using an optical diametric transducer to measure the instantaneous minimum diameter of hourglass-shaped cylindrical specimens. Meyer and Pruitt [13] measured the axial strains from the distance between two grid lines spaced about 2.5 mm along the axial direction to investigate the effect of cyclic true strain on the morphology, structure and relaxation behavior of

* Corresponding author. Tel./fax: +86 29 82665168.
E-mail addresses: fangqz@mail.xjtu.edu.cn (Q.-Z. Fang), wangtj@mail.xjtu.edu.cn (T.J. Wang).

0032-3861/$ - see front matter © 2006 Elsevier Ltd. All rights reserved.
doi:10.1016/j.polymer.2006.04.069

polyethylene with ultra high molecular weight. Gloaguen and Lefebvre [14] studied the plastic deformation of nylon 6/clay and polypropylene/clay nanocomposites, in which the volume strain was recorded by video-extensometry. G'Sell et al. [15] developed a special video-controlled tensile testing system to measure the stress–strain relation and the volume changes of PET and HIPS polymers, in which seven ink markers were printed on the front surface prior to deformation and analyzed during the tensile test in order to characterize the local plastic deformation. Bai and Wang [16] used a similar method as G'Sell et al. [15] to study the plastic damage mechanisms of PP/PA6/POE blends under cyclic tension.

More recently, digital image correlation (DIC) analysis method is successfully employed to measure the large deformation of polymers and appears its advantages. Based on DIC analysis and using a non-contact and non-intrusive digital speckle laser extensometry, Laraba-Abbes et al. [17] developed a methodology for the large deformation measurement of rubber-like materials, then obtained the two-dimensional in-plane displacement components using a coarse-fine search method and carried out local strain measurements of carbon black filled natural rubber. Based on DIC analysis and the associated data reduction schemes, Parsons et al. [18] developed a tool for the measurement of the large strain behavior of an inhomogeneous deforming glassy polymer and successfully measured tensile stress–strain behavior full-field strain contours and volumetric strain. In the testing procedure of Parsons et al. [18], an artificial random speckle pattern was applied with ink to the surface of rectangular bar-type PC specimens, the pattern density was maximized under the constraint that individual speckles should generally not overlap and the minimum characteristic speckle size was three pixels.

In this study, the DIC method is used to measure, in three dimensions, the large inhomogeneous deformation of PC/ABS alloy during a standard uniaxial tension test. Two CCD cameras are used to simultaneously acquire digitalized images of the specimen surfaces in the two lateral directions, respectively, during a tensile test. The inhomogeneous incremental displacement fields in the two lateral directions are calculated by correlating the subsets in reference images to the subsets in deformed images, the total displacement fields are obtained by the summation of the incremental displacement fields, and then the true stress–strain behavior and volume variation of PC/ABS alloy are calculated from the total displacement fields. Moreover, SEM in situ observation is carried out to investigate the micro-mechanism of tensile deformation of PC/ABS alloy.

2. Experimental

2.1. Material and specimens

The polymeric material used in this study is PC/ABS alloy with blending ratio 70/30 of PC to ABS. The average molecular weight of PC is 26000. ABS has different pellet sizes and consists mainly of 0.2–0.5 μm in diameters. The blend is injected into dumb-bell tension specimen with dimensions shown in Fig. 1(a). Injection temperature and holding pressure are 240–250 °C and 60–80 MPa, respectively. Dimensions of the gage region of the specimen are 70 mm × 10 mm × 4 mm. The specimen used for SEM in situ observation is shown in Fig. 1(b).

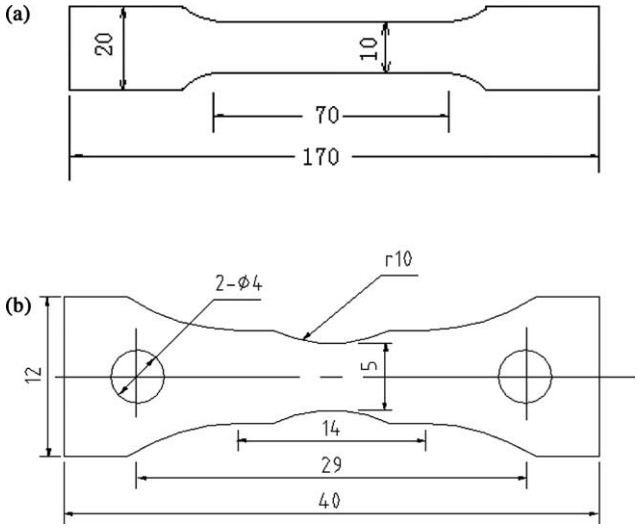

Fig. 1. Geometry and dimensions of specimens. (a) Specimen with thickness of 4 mm for tensile tests and (b) specimen with thickness of 1.2 mm for SEM dynamic tensile tests.

2.2. Displacement measurement

Fig. 2 shows two of the images obtained during testing. One is reference image and the other is deformed image. Choose a region to be measured from the reference image, in which point $D(x_i,y_j)$ is an arbitrary point. To calculate the values of

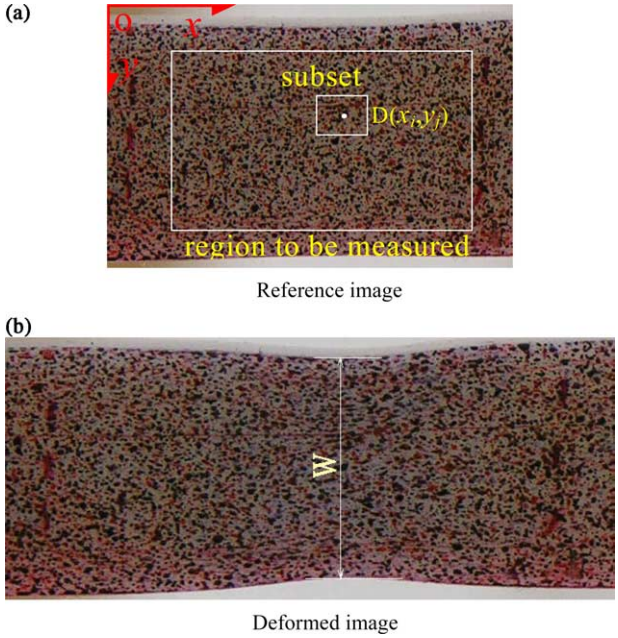

Fig. 2. Reference and deformed images with W being the minimum width of specimen.

displacements of point $D(x_i,y_j)$, a small subset with dimensions $(2n+1)$ pixels$\times(2n+1)$ pixels is chosen around D. The value of n could be chosen as 5–20, according to the quality of the random speckle pattern on the specimen surface. The discrete matrix of the values of pixel color (RGB) in the subset forms a unique pattern within the image. If we take $f_1(x,y)$ and $f_2(x,y)$ as the character functions of the reference and deformed images, respectively, and the displacement functions as $u(x,y)$ and $v(x,y)$, then the characteristic color value at point (x,y) in the reference image should be the characteristic color value at point $(x+u,y+v)$ in the deformed image, i.e.

$$f_1(x,y) = f_2[x + u(x,y), y + v(x,y)] \tag{1}$$

If we represent $f_1(x,y)$ and $f_2(x,y)$ with the discrete values $f_1(x_i,y_j)$ and $f_2(x_i,y_j)$, respectively, then the crosscorrelation coefficient C could be calculated as

$$C=\frac{\sum_{k=-n}^{n}\sum_{l=-n}^{n} f_1(x_i+k,y_j+l)f_2(x_i+k+u,y_j+l+v)}{\sqrt{\sum_{k=-n}^{n}\sum_{l=-n}^{n} f_1^2(x_i+k,y_j+l)}\sqrt{\sum_{k=-n}^{n}\sum_{l=-n}^{n} f_2^2(x_i+k+u,y_j+l+v)}} \tag{2}$$

If $C=1$, the subset considered in the reference image will completely correlate with that in the deformed image. If $C=0$, there are no correlation between them. Generally, if C takes the maximum value for a set of (u,v) in a reasonable collection of displacements, then the values of (u,v) would most likely be the true displacement at point (x_i,y_j). Searching the whole measured region, one can obtain the displacement fields on the region to be measured. If one takes the deformed image as reference image, the incremental displacement fields can be obtained. The total displacement fields are obtained with the summation of the incremental displacement fields. Moreover, the true axial and shear strains can be calculated from the displacement fields. Generally, the displacement fields could be calculated with a subset size of (10–40)$\times$(10–40) depending on the accuracy needed and the quality of random speckle pattern on the specimen surfaces.

The principal features and procedures of displacement measurement system developed in this paper are shown in Fig. 3.

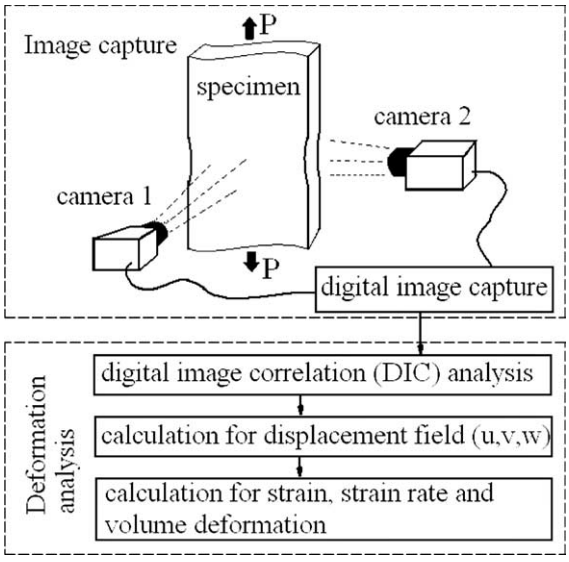

Fig. 3. Block diagram of the deformation measurement system.

2.3. Uniaxial tensile tests

Using the plate specimens, as shown in Fig. 1(a), uniaxial tensile tests are carried out following the ASTM D-638 standard test method at room temperature of approximate 23 °C. The testing machine chosen is a universal machine, MTS-858. Crosshead speed of the testing machine is 1 mm/min. Three dimensional deformations in the axial, width and thickness directions are recorded through two cameras with high resolutions (3264 pixels$\times$2448 pixels and 2776 pixels$\times$2074 pixels, respectively), respectively, at regular intervals of about 30 s during a tensile test, as shown in Fig. 3. Resolutions of the pictures are 46 pixels/mm in longitudinal and width directions, and 32 pixels/mm in thickness direction of the specimen. To keep the synchronization of the photographs with the load data, efforts are made to insure the loading and two cameras being started simultaneously. To ensure each specimen necking within the gage length, thickness near the center of the specimen is reduced by 0.1 mm with fine sand paper. This is an effective method to locate the necking place and has no obvious effect on the successive deformations after necking.

To give a better characterization of the specimen surfaces, random speckle pattern with three different colors (black, blue and red) is applied to each specimen surfaces.

2.4. SEM in situ observation

The really micro-processes of deformation of PC/ABC are observed directly through in situ observation. The specimen used is shown in Fig. 1(b) and is loaded in a scanning electron microscope (JEOL, JSM-35C) with maximum load capacity of 5 kN. All the tests are performed at room temperature. The actual deformation processes are recorded with SEM photographs.

3. Results and discussion

3.1. Displacement fields

Fig. 4 shows three images of PC/ABS specimen recorded at different stages of deformation. It is seen that necking occurs at relative small strain, and then grows along the axial direction of specimen. For most PC/ABS specimens, necking extends to the shoulders of the specimen, after then the specimen breaks. But, some specimens break before the necking regions reach to the shoulders of specimen. Through DIC analysis, we obtain the incremental displacement fields, and obtain the total displacement field at different deformation stage. Fig. 5(a) and (b) show the axial and lateral

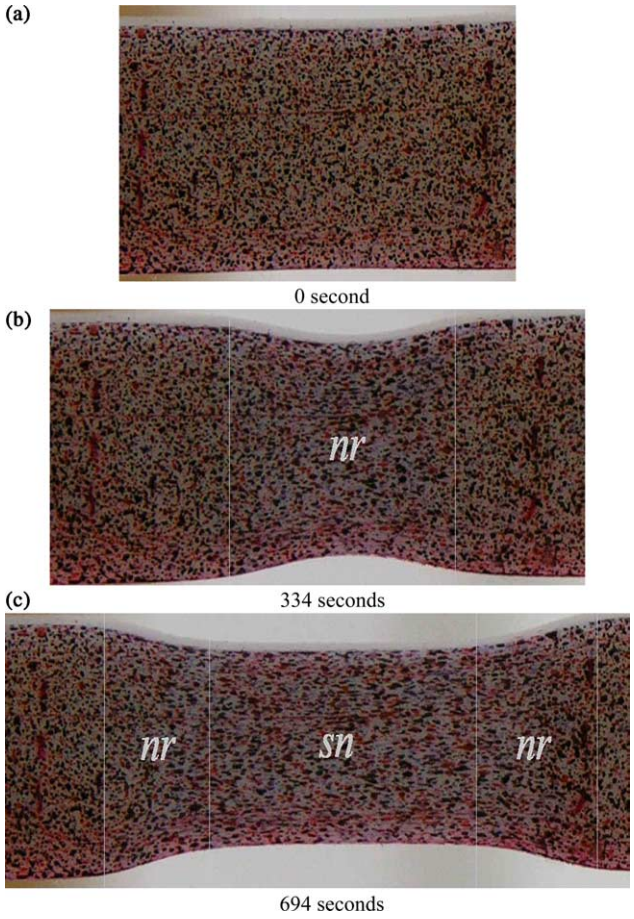

Fig. 4. Front view images of PC/ABS tensile specimen at different time. (a) Image at 0 s, (b) and (c) images at 334 and 694 s, respectively. Where nr and sn are necking and stable necking regions.

displacement fields $u(x,y)$ and $v(x,y)$ for a PC/ABS specimen at time = 334 s, respectively, in which x and y are the pixel coordinates in the undeformed (reference) image as shown in Fig. 2. The unit of the displacements u and v is pixel. It is seen that necking occurs at this stage and shear deformation is almost symmetric. Variations of u and v are great too at this stage.

To evaluate the accuracy of the DIC method, variation of the minimum width w shown in Fig. 2(b) at different deformation stage is measured manually with professional image processing software Image-pro-plus 4.5.1. Comparison of the width ratio w/w_0 measured from DIC and the manual methods at different time is shown in Fig. 6, in which w and w_0 are the instantaneous minimum and initial width of specimen, respectively. It is seen that the measurement result of DIC method is in excellent agreement with the result of manual method.

3.2. Strain

The main purpose of this paper is to obtain the stress–strain relation of PC/ABS alloy. It is unnecessary to calculate the strain fields. The maximum axial strain and the minimum crosssection area at different deformation stage are required

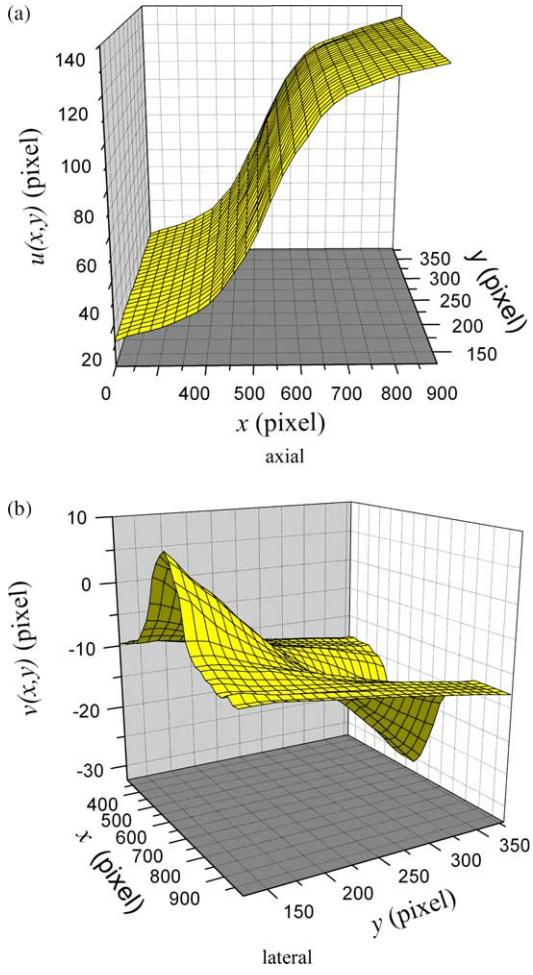

Fig. 5. Displacement fields at 334 s. Displacement fields $u(x,y)$ and $v(x,y)$ in axial (a) and lateral (b) directions, respectively.

to calculate the true stress, and true strain could be obtained with the axial displacement nearby. It is seen from experiment that the axial deformation is nearly uniform in any section of the specimen, as shown in Fig. 5(a). That is, the values of $u(x,y)$ are nearly constant for a fixed x. Therefore, it is reasonable to represent the axial strain of the specimen with the average value of the maximum tensile strain of the middle lines on the surfaces in width and the thickness directions of the specimen.

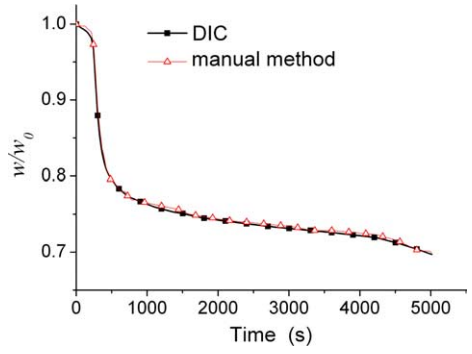

Fig. 6. Contraction ratios (w/w_0) measured from DIC and manual methods.

Let $u_w(x)$ and $u_t(x)$ be the axial displacements of the center lines on the width and thickness surfaces of the specimen, respectively, then the maximum tensile engineering strains in the two lateral directions can be calculated as

$$\varepsilon_e^w = \left(\frac{du_w}{dx}\right)_{max} \tag{3}$$

$$\varepsilon_e^t = \left(\frac{du_t}{dx}\right)_{max} \tag{4}$$

and the average axial tensile engineering strain can be expressed as

$$\varepsilon_e = \frac{\varepsilon_e^w + \varepsilon_e^t}{2} \tag{5}$$

Similarly, the maximum tensile true strains in the two lateral directions can be calculated as

$$\varepsilon_{true}^w = \ln\left[1 + \left(\frac{du_w}{dx}\right)_{max}\right] \tag{6}$$

$$\varepsilon_{true}^t = \ln\left[1 + \left(\frac{du_t}{dx}\right)_{max}\right] \tag{7}$$

and the average axial tensile true strain can be expressed as

$$\varepsilon_{true} = \frac{\varepsilon_{true}^w + \varepsilon_{true}^t}{2} \tag{8}$$

According to the displacement field at different time, the variations of the maximum axial engineering strain ε_e and the maximum axial true strain ε_{true} with time are obtained, as shown in Fig. 7. Generally, the deformation is homogeneous before yielding. However, necking occurs after yielding and propagates in the axial direction with the increase of deformation, as shown in Fig. 4, which results in the inhomogeneous deformation of material. The strain rate is high in the necking region nr, but it decreases to very low level in the stable neck region sn, as shown in Fig. 4. The strain rate of the maximum true axial strain is nearly a constant at the first, and jumps an order of magnitude as neck forms, then decreases greatly to low positive values with time, as shown in Fig. 8. Variation of the strain rate

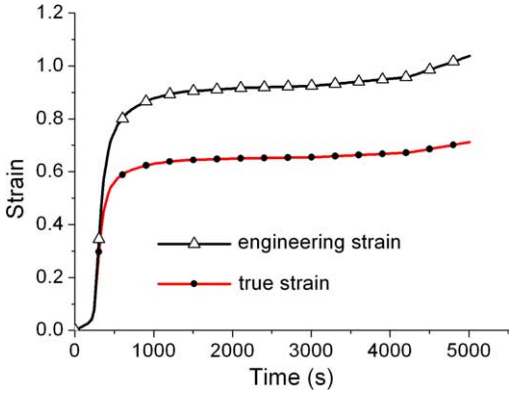

Fig. 7. Maximum tension strain vs time.

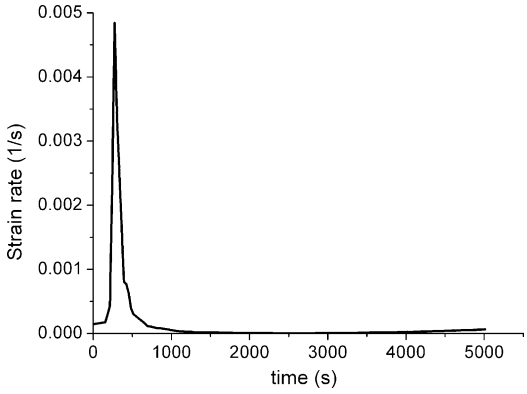

Fig. 8. Strain rate at minimum section of the specimen.

with true axial strain is shown in Fig. 9. It is seen that the strain rate is almost a constant at the stage of elastic deformation, and increases rapidly at first during plastic deformation, and then decreases gradually with the increase of deformation.

3.3. Volume variation

Let $v_w(y)$ and $v_t(y)$ be the lateral displacements in width and thickness directions, respectively, at the minimum cross-sections of the specimen, then the width ratio w/w_0 and thickness ratio t/t_0 can be calculated as

$$\frac{w}{w_0} = 1 + \frac{dv_w}{dy} \tag{9}$$

$$\frac{t}{t_0} = 1 + \frac{dv_t}{dy} \tag{10}$$

From Eqs. (9) and (10), we obtain the following expression of the variation of local volume of the specimen

$$\frac{V}{V_0} = \left(\frac{w}{w_0}\frac{t}{t_0}\right)(1 + \varepsilon_e) \tag{11}$$

where V and V_0 are the instantaneous and reference values of local volume, respectively.

From Eqs. (9) and (10), we can also calculate the true strains in the width and thickness directions

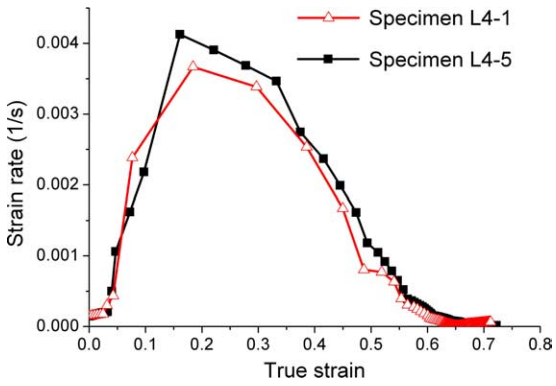

Fig. 9. Strain rate vs axial true strain measured from different specimens.

$$\varepsilon^{w}_{\text{lateral}} = \ln\left(\frac{w}{w_0}\right) \tag{12}$$

$$\varepsilon^{t}_{\text{lateral}} = \ln\left(\frac{t}{t_0}\right) \tag{13}$$

The average value of the lateral true strain can be expressed as

$$\varepsilon_{\text{lateral}} = \frac{\varepsilon^{w}_{\text{lateral}} + \varepsilon^{t}_{\text{lateral}}}{2} \tag{14}$$

Substituting Eqs. (12) and (13) into Eq. (14), we have

$$\varepsilon_{\text{lateral}} = \frac{1}{2}\ln\left(\frac{A}{A_0}\right) \tag{15}$$

where

$$\frac{A}{A_0} = \left(\frac{w}{w_0}\,\frac{t}{t_0}\right) \tag{16}$$

with A and A_0 being the instantaneous and initial values of the area of the minimum crosssection of the specimen. We define the effective Poisson's ratio as

$$\mu_{\text{eff}} = -\frac{\varepsilon_{\text{lateral}}}{\varepsilon_{\text{true}}} \tag{17}$$

Substituting Eqs. (8) and (15) into Eq. (17), we have

$$\mu_{\text{eff}} = -\frac{1}{2\varepsilon_{\text{true}}}\ln\left(\frac{A}{A_0}\right) \tag{18}$$

Variations of the ratios w/w_0 and t/t_0 of the PC/ABS specimen with time are shown in Fig. 10. It is seen that contraction in the two lateral directions of the specimen is homogeneous as the deformation is small, but the contraction of the thickness of the specimen is larger than that of the width of the specimen at the later plastic stage of deformation. It may be induced by the inhomogeneous deformation properties of the material or due to the different constraints in the width and thickness directions.

It is well known that volume deformation is an important phenomenon for polymers. G'Sell et al. [15] and Parsons et al. [18] have measured the volume variations of different polymers through different methods. Using the DIC method, we obtain the volume variation of PC/ABS alloy with the true axial strain, as shown in Fig. 11. It is seen that the ratio

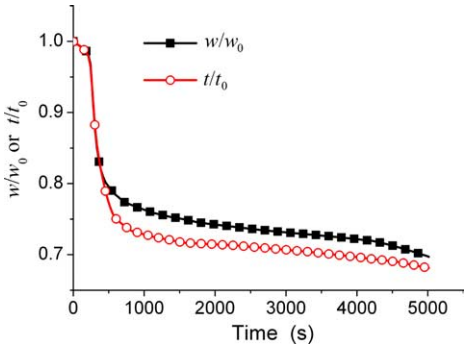

Fig. 10. Contraction ratios of thickness (t/t_0) and width (w/w_0) of specimen.

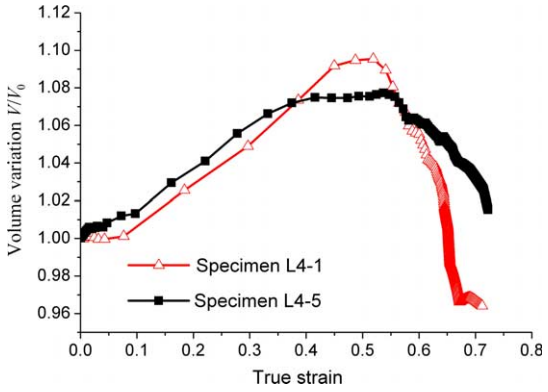

Fig. 11. Volume variation of PC/ABS alloy with true axial strain during loading measure from different specimens.

V/V_0 increases with the increase of true axial strain, which is in agreement with [15,18], and then decreases with increasing the true axial strain, which is not seen in literatures. One can see from Fig. 9 that the strain rate decreases to a lower value as the true axial strain reaches to approximate 0.5 that just corresponds to the starting of the decrease of V/V_0. For the high value of strain and the low value of strain rate, molecular chains slide more sufficiently and the entanglements release more easily. In this case, the voids formed in the early stage of deformation might close, which may result in the decrease of V/V_0. At large deformation stage, the molecular chains might be reoriented [13] and the density of polymer could increase [19]. The

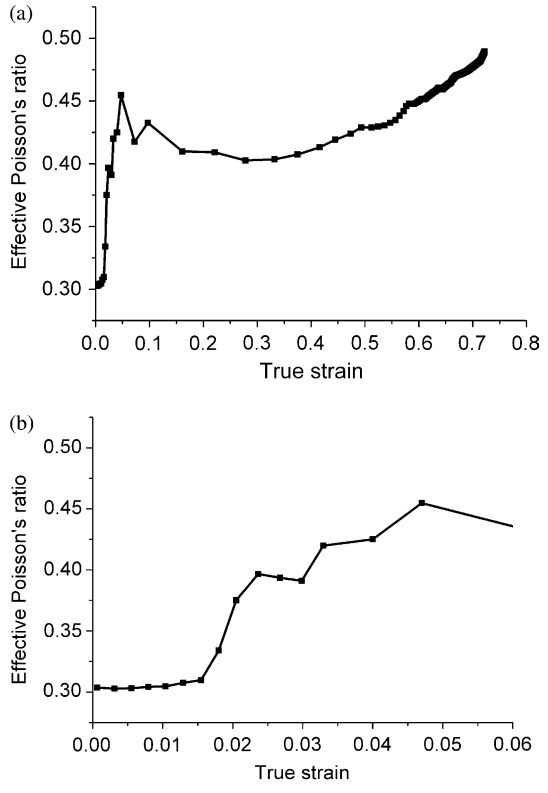

Fig. 12. Effective Poisson's ratio vs axial true strain (a) and partially enlargement of (a).

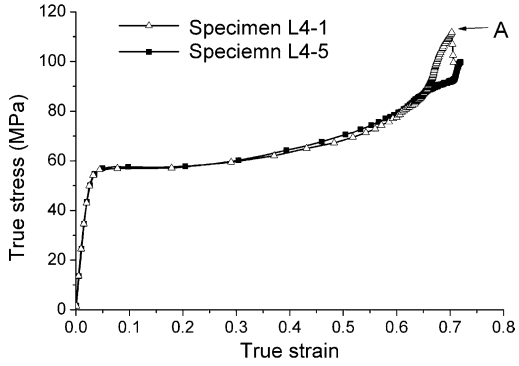

Fig. 13. True stress–strain curves of PC/ABS alloy measured from different specimens.

other reasons to result in the decrease of V/V_0 should be the further investigation.

Poisson's ratio is another important mechanical parameter of polymer. Fig. 12 shows the variation of the effective Poisson's ratio μ_{eff} of PC/ABS alloy defined in Eq. (17) with true axial strain. It is seen that the effective Poisson's ratio μ_{eff} is almost a constant (approximate 0.305–0.309) in the stage of elastic deformation, as shown in Fig. 12(b), and varies in a small region of 0.408–0.488 with the true axial strain in the stage of plastic deformation, as shown in Fig. 12(a). It is shown from Figs. 11 and 12 that the increase of the effective Poisson's ratio μ_{eff} during orientation strengthening deformation stage of the specimen might correspond to the decrease of the V/V_0.

3.4. True stress–true strain curves

The true stress is defined as

$$\sigma_{\text{true}} = \frac{P}{wt} = \frac{P/w_0t_0}{(w/w_0)/(t/t_0)} \tag{19}$$

where P is force, w_0 and t_0 are the width and thickness within the gage of the specimen measured before test. Substituting Eqs. (9) and (10) into Eq. (19), we can calculate the true stress in the specimen. Considering Eqs. (8) and (19), we can plot the true stress–strain curves of PC/ABS alloy measured from different specimens, as shown in Fig. 13. It is seen that there is no obvious strain softening for the PC/ABS alloy, and obvious strain hardening can be seen. It should be pointed out that the stress relaxation occurs at point A for specimen L4-1.

3.5. Micromechanism of deformation of PC/ABS alloy

From the SEM in situ observation to small specimen shown in Fig. 1(b), we obtain the process of deformation of PC/ABS alloy. A typical example is shown in Fig. 14, from which one can see the crazing process in PC/ABS alloy. Here, crazing initiates from the original micro defects (voids or cracks) on the surface of the specimen. With the increase of deformation, the original micro defects grow up and new ones initiate. After yielding, clear crazing structures can be seen, as shown in Fig. 14(c), and it become more clearly and its density increases with the increase of plastic deformation, as shown in Fig. 14(d). However, because some of the gold layer in the craze structures is broken, the crazes in Fig. 13(c) looks like white structures. After sputtering a thin gold layer on the specimen surface again, the crazing structures are clearly shown in Fig. 14(d). The enlarged micro structure of craze is shown in Fig. 15, from which one can seen although some of the crazes are not perpendicular to the tensile direction, the fibrils in the crazes are mainly parallel with the tensile direction.

4. Conclusion

The large tensile deformation behavior of PC/ABS alloy is experimentally investigated. Based the DIC method, we

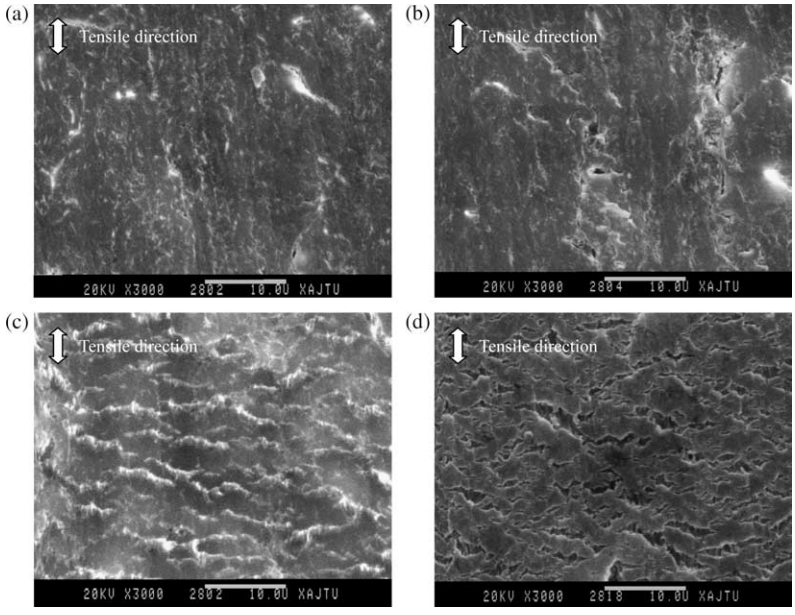

Fig. 14. Typical process of deformation of PC/ABS alloy. (a) Undeformed, (b) just before yielding, (c) just after yielding (the gold layer was broken) and (d) post-yielding (sputtering gold layer again).

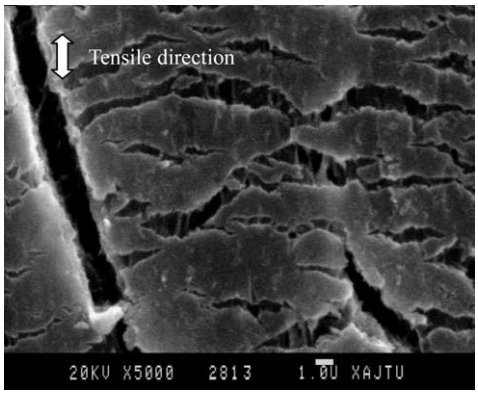

Fig. 15. Craze structures in PC/ABS alloy at the stage of large plastic deformation.

developed a measurement system for the three-dimensional inhomogeneous large deformation of polymers. The validity of the deformation measuring method is verified in this paper.

The true stress–strain curve of PC/ABS alloy is obtained. It is shown that no obvious stress softening occurs for the material in terms of true stress–strain relations. The variations of volume and Poisson's ratio with axial true strain are given. It is seen that the ratio V/V_0 increases and then decreases with the increase of the true axial strain, which is not seen in literatures. The contraction in the two lateral directions of the specimen is homogeneous as the deformation is small, but the thickness contraction is larger than that of the width at the later stage of deformation. From SEM in situ observation, we obtain the crazing process during the tensile deformation of PC/ABS alloy.

Acknowledgements

This work is supported by the National Natural Science Foundation of China (10125212 and 10472087) and the MOE Key Project. Nanjing Julong Engineering Plastics Corporation is acknowledged for providing the PC/ABS alloy.

References

[1] O'Connel PA, Bonner MJ, Duchekтt RA, Ward IM. Polymer 1995;36:2355–62.
[2] Li XW, Hristov HA, Yee AF. Polymer 1995;36:759–65.
[3] Wang TJ, Kishimoto K, Notomi M. Key Eng Mater 2000;183/187:121–6.
[4] Notomi M, Kishimoto K, Wang TJ, Shibuya T. Key Eng Mater 2000;183/187:779–84.
[5] Wang TJ, Kishimoto K, Notomi M. Acta Mechanica Sinica 2002;18(5):480–93.
[6] Ramaswamy S, Lesser AJ. Polymer 2002;43:3743–52.
[7] Rizzieri R, Baker FS, Donald AM. Polymer 2003;44:5927–35.
[8] Chen HB, József KK, Wu JS. Polymer 2004;45:6375–82.
[9] Richeton J, Schlatter G, Vecchio KS, Rémond Y, Ahzi S. Polymer 2005;46:8194–201.
[10] Buisson G, Ravichandar K. Polymer 1989;31:2071–6.
[11] Haynes AR, Coates PD. J Mater Sci 1996;31:1843–55.
[12] G'Sell C, Hiver JM, Dahoun A, Souahi A. J Mater Sci 1992;27:5031–9.
[13] Meyer RW, Pruitt LA. Polymer 2001;42:5293–306.
[14] Gloaguen JM, Lefebvre JM. Polymer 2001;42:5841–7.
[15] G'Sell C, Hiver JM, Dahoun A. Int J Solid Struct 2002;39:3857–72.
[16] Bai SL, Wang M. Polymer 2003;44:6537–47.
[17] Laraba-Abbes F, Ienny P, Piques R. Polymer 2003;44:3883–91.
[18] Parsons E, Boyce MC, Parks DM. Polymer 2004;45:2665–84.
[19] Brady TE, Yeh GSY. J Appl Phys 1971;42(12):4622–30.